Published online 13 April 2020

Nucleic Acids Research, 2020, Vol. 48, No. 9 ***5119–5134***
doi: 10.1093/nar/gkaa193

Mutagenesis mechanism of the major oxidative adenine lesion 7,8-dihydro-8-oxoadenine

Myong-Chul Koag†, Hunmin Jung† and Seongmin Lee*

The Division of Chemical Biology and Medicinal Chemistry, College of Pharmacy, The University of Texas at Austin, Austin, TX 78712, USA

Received January 21, 2020; Revised March 06, 2020; Editorial Decision March 10, 2020; Accepted April 07, 2020

ABSTRACT

Reactive oxygen species generate the genotoxic 8-oxoguanine (oxoG) and 8-oxoadenine (oxoA) as major oxidative lesions. The mutagenicity of oxoG is attributed to the lesion's ability to evade the geometric discrimination of DNA polymerases by adopting Hoogsteen base pairing with adenine in a Watson–Crick-like geometry. Compared with oxoG, the mutagenesis mechanism of oxoA, which preferentially induces A-to-C mutations, is poorly understood. In the absence of protein contacts, oxoA:G forms a wobble conformation, the formation of which is suppressed in the catalytic site of most DNA polymerases. Interestingly, human DNA polymerase η (polη) proficiently incorporates dGTP opposite oxoA, suggesting the nascent oxoA:dGTP overcomes the geometric discrimination of polη. To gain insights into oxoA-mediated mutagenesis, we determined crystal structures of polη bypassing oxoA. When paired with dGTP, oxoA adopted a *syn*-conformation and formed Hoogsteen pairing while in a wobble geometry, which was stabilized by Gln38-mediated minor groove contacts to oxoA:dGTP. Gln38Ala mutation reduced misinsertion efficiency ∼55-fold, indicating oxoA:dGTP misincorporation was promoted by minor groove interactions. Also, the efficiency of oxoA:dGTP insertion by the X-family polβ decreased ∼380-fold when Asn279-mediated minor groove contact to dGTP was abolished. Overall, these results suggest that, unlike oxoG, oxoA-mediated mutagenesis is greatly induced by minor groove interactions.

INTRODUCTION

Numerous endogenous (e.g. oxidative phosphorylation) and exogenous (e.g. ultraviolet rays) sources produce reactive oxygen species (ROS) such as hydrogen peroxide and hydroxyl radicals. ROS are latent or potent electrophiles that can damage DNA to generate a wide spectrum of genotoxic lesions, including 7,8-dihydro-8-oxoguanine (oxoG) and 7,8-dihydro-8-oxoadenine (oxoA), which are implicated in cancer development, neurodegeneration, and aging (Figure 1A) (1). The higher genotoxicity of oxoG, a ubiquitous lesion found in physiological DNA, is well established both *in vitro* and *in vivo* (2). The mutagenicity of oxoG is attributed to the lesion's dual coding properties at the replicating site of DNA polymerases. Structural studies show that templating *syn*-oxoG uses its Hoogsteen edge to base pair with incoming *anti*-dATP (3–6). In the oxoG:dATP base pair, the O6 and N7-H of oxoG engage in hydrogen bonds with the N6-H and N1 of dATP, respectively. The base pairing geometry of oxoG:dATP in the polymerase active site is virtually identical to that of the undamaged correct base pair (Figure 1B), thereby evading the geometric constraints imposed by the catalytic-site architecture of DNA polymerases (3,4). The facile formation of the Watson–Crick-like oxoG:dATP in the nascent base pair site thus promotes G-to-T transversions.

Compared with the major oxidative guanine lesion oxoG, the major oxidative adenine lesion oxoA has been much less investigated. OxoA, of which the cellular levels are one-third to one-half of those of oxoG (7,8), is found in irradiated DNA and human cancerous tissues (7,9–11). While oxoG is removed by the so-called 'GO' system that employs oxoguanine DNA glycosylase (e.g. hOGG1, MutM) and adenine DNA glycosylase (e.g. hMYH, MutY), oxoA opposite thymine is excised by *Escherichia coli* mismatch-specific uracil DNA glycosylase (MUG) and human thymine DNA glycosylase (TDG) (1,12–14). In the absence of protein contacts, unlike oxoG, which forms a Watson–Crick-like base pair with dA, *syn*-oxoA forms a wobble base pair with *anti*-dG (Figure 1C) (15), where the O8 and N7-H of oxoA are hydrogen bonded to the N1-H and O6, respectively.

The mutagenic properties of the major oxidative adenine lesion oxoA remain poorly understood. OxoA is almost non-mutagenic in bacterial cells (16). In mammalian cells, however, the same lesion displays mutagenicity comparable to that of oxoG (17,18), suggesting a differential mecha-

*To whom correspondence should be addressed. Tel: +1 512 471 1785; Fax: +1 512 471 4726; Email: seongminlee@austin.utexas.edu
†The authors wish it to be known that, in their opinion, the first two authors should be regarded as Joint First Authors.

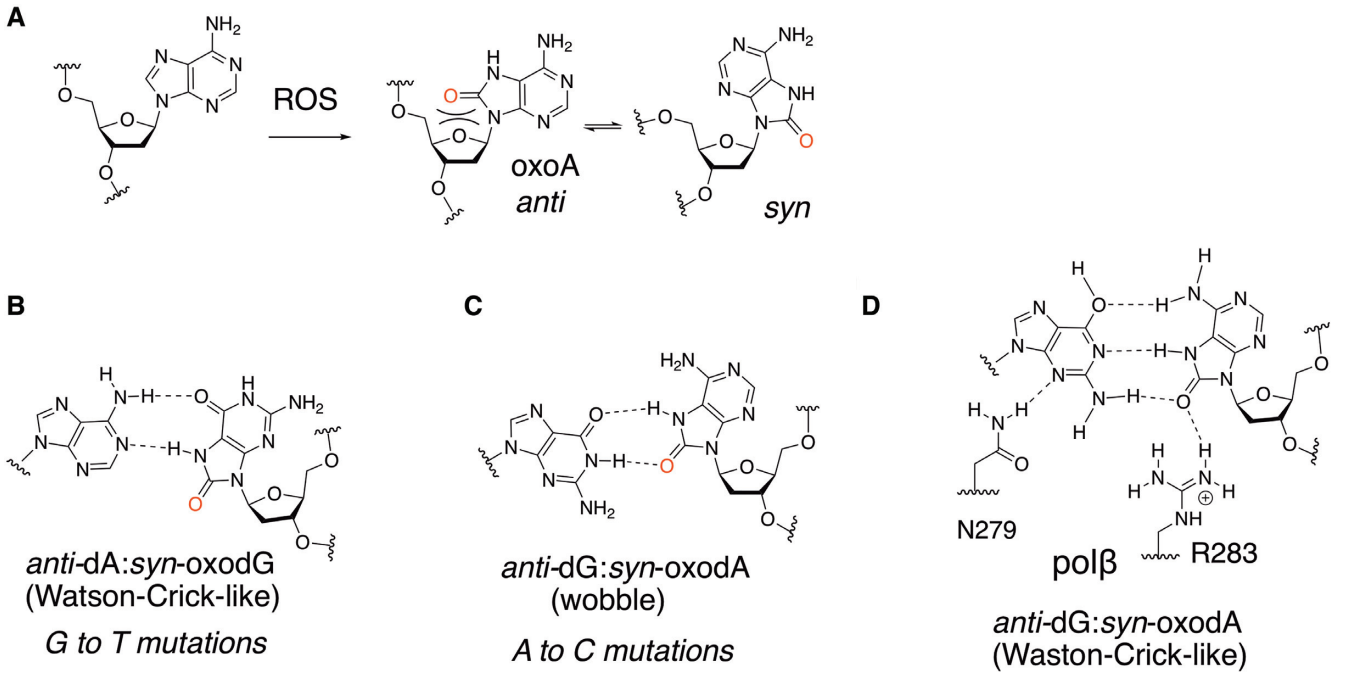

Figure 1. Base pairing properties of 7,8-dihydro-8-oxoguanine (oxoG) and 7,8-dihydro-8-oxoadenine (oxoA) in duplex DNA. (**A**) Generation of oxoA by ROS. Structures of *syn* and *anti* conformers of oxoA. (**B**) Base pairing of *syn*-oxoG:*anti*-A. OxoG and dA form Hoogsteen hydrogen bonds with Watson–Crick-like geometry. (**C**) Base pairing of *syn*-oxoA:*anti*-G. OxoA and dG form Hoogsteen hydrogen bonds with a wobble geometry. (**D**) Base pairing of *syn*-oxoA:*anti*-G in the active site of polβ. In the polβ catalytic site, s*yn*-oxoA and *anti*-G form three hydrogen bonds with Watson–Crick-like base-pair conformation. Minor groove contacts by polβ are shown.

nism of mutagenicity of the major oxidative adenine lesion. While prokaryotic DNA polymerases (e.g. *E. coli* DNA polymerase I) bypass oxoA in an error-free manner (19,20), mammalian DNA polymerases (pols α, β and η) frequently incorporate dGTP opposite the lesion (17). In particular, human Y-family DNA polymerase η (polη) inserts dGTP opposite oxoA >60-fold more efficiently than opposite dA and readily extends across oxoA:dG (21). The presence of oxoA at a templating position decreases the replication fidelity by ∼100-fold, facilitating mutagenic replication. Also, human X-family DNA polymerase β (polβ) incorporates dGTP opposite oxoA ∼400-fold more efficiently than dA (21). Crystal structures of polβ in complex with templating oxoA show the oxidative lesion forms Watson–Crick base pairing with dTTP and Hoogsteen pairing with dGTP (Figure 1D) (21). In polβ active site, oxoA and dG form three hydrogen bonds with Watson–Crick-like geometry (Figure 1D), suggesting polymerase contacts induce the mutagenic oxoA:dGTP base-pair conformation. OxoA is more likely to be bypassed by translesion synthesis (TLS) DNA polymerases rather than by the base excision repair protein polβ. Therefore, the structure of TLS polymerase in complex with oxoA is needed for a better understanding of oxoA-mediated mutagenesis, yet such structure has not been reported.

Polη, a Y-family TLS DNA polymerase, is specialized for bypassing UV light-induced cyclobutane pyrimidine dimers (CPD) (22,23). Mutations in the *POLH* gene causes the variant form of xeroderma pigmentosum, which increases the rates of skin and internal cancers. In addition to CPD, the enzyme has been implicated in the bypass of various DNA lesions, including cisplatin-GG adducts (24,25), abasic sites, O6-methylguanine, and oxoG (26), among others (27,28). In particular, polη plays a major role in the bypass of oxoG in yeast (29). Unlike high-fidelity DNA polymerases that frequently misincorporate dATP opposite oxoG, polη accurately and efficiently replicates across oxoG *in vitro* (26,30–32). In yeast, oxoG is not bypassed by polε at the normal S-phase dNTP concentration (33) but is inefficiently and inaccurately bypassed by polδ (29,34). The inefficient bypass of oxoG by these replicative DNA polymerases may result from the sensitivity of high-fidelity polymerases toward the conformational change in the sugar-phosphate backbone induced by the 8-oxo moiety of oxoG (35,36). Bypass of oxoA by replicative DNA polymerases has not been reported so far. However, the significant conformational distortion in the phosphate backbone triggered by oxoA (35) suggests that the major oxidative adenine lesion would be a significant block to catalysis by high-fidelity DNA polymerases and, if not removed, would be bypassed by TLS DNA polymerases such as Polη.

To gain insights into oxoA-mediated mutagenesis in human cells, we have solved crystal structures of human polη incorporating dGTP or dTTP opposite oxoA. We also present kinetic data and a ternary structure of Gln38Ala polη mutant bypassing oxoA. To further our understanding of the promutagenic replication of oxoA by polβ, we have conducted kinetic and structural studies of Asn279Ala polβ mutant inaccurately bypassing oxoA. These results reveal new insights into the promutagenic mechanism of the major oxidative adenine lesion in humans.

MATERIALS AND METHODS

Polη expression and purification

The catalytic core of human polη (residues 1–432) was cloned into pET28a plasmid with NcoI and BamHI restriction enzyme sites. Polη and Gln38Ala polη were overexpressed in *E. coli* BL21 (DE3) cells. Cultures were grown in Luria-Bertani medium at 37°C until reaching the OD_{600} of 0.6, and the cells were induced by adding isopropyl β-D-α-thiogalactopyranoside (0.3 mM). After 18 h incubation at 20°C, the pelleted cells were resuspended in Ni–NTA column binding buffer A (50 mM sodium phosphate, pH 7.8, 500 mM NaCl and 10% glycerol) supplemented with 1 mg/ml lysozyme, 0.25% NP-40, 0.25% Triton X-100 and 0.25 mM phenylmethylsulfonyl fluoride. After sonication for 60 s, the lysate was centrifuged at 15 000 *g* at 4°C for 20 min. The supernatant was then purified by using Ni–NTA column (GE Healthcare). The Ni-NTA column purification was conducted with a linear gradient of 10–500 mM of imidazole over 8 column volumes. The imidazole-eluted fractions from the Ni-NTA column were combined and further purified using the Heparin HiTrap column (GE Healthcare) followed by Superdex-75 size exclusion chromatography (GE Healthcare). Heparin HiTrap column purification was carried out over 15 column volumes with a linear gradient of 0.1–1 M NaCl in 50 mM Tris·HCl pH 7.4, 5 mM β-ME, and 10% glycerol. The proteins were stored at 9 mg/ml in a size exclusion chromatography buffer (50 mM Tris, pH 7.5, 450 mM KCl, 10% glycerol and 3 mM dithiothreitol), flash-frozen in liquid nitrogen and stored at −80°C.

Plasmid construction of Gln38Ala mutant of human polη and Asn279Ala mutant of human polβ

The Gln38Ala mutant of human polη and the Asn279Ala mutant construct of polβ and were prepared using the manufacturer's protocol for the Quikchange Mutagenesis System (Stratagene), which employs the oligonucleotide-directed mutagenesis. For Gln38Ala polη preparation, a forward primer (5′-GCCTTTCCATGATTTATACGC AACCACGGCGCACGGTTT-3′) and a reverse primer (5′-AAACC GTGCGCCGTGGTTGCGTATAAATC ATGGAAAGGC-3′) were used to generate a single mutant Gln38Ala polη. For Asn279Ala mutant polβ construct preparation, a pair of complementary mutagenic oligonucleotides, (forward) 5′-CACTGGGAGTGAT ATTTTCGCTAAGAATATGAGGGCTCATG-3′ and (reverse) 5′-CATGAGCCCTCATATTCTTAGCGAAA ATATCACTCCCAGTG-3′, were designed to introduce a mutant codon (underlined) encoding Asn279Ala mutation in the polβ sequence. The DNA sequence of the desired construct was confirmed by DNA sequencing (DNA Core Facility, the University of Texas at Austin).

Crystallization and structure determination of Asn279Ala polβ

To obtain the ternary complex of Asn279Ala polβ-DNA complex, a 10-fold molar excess of non-hydrolyzable dGMPNPP (Jena Bioscience) was added to the binary complex, which was prepared by mixing polβ with a single-nucleotide gapped DNA containing a 16-mer template (5′-CCGAC(oxoA)GCGCATCAGC-3′), a complementary 10-mer upstream primer (5′-GCTGATGCGC-3′), and a 5-mer downstream primer (5′-pGTCGG-3′) in a 1:1.2 molar ratio. Ternary polβ-DNA complex co-crystals with the non-hydrolyzable dGTP analog paired with templating oxoA were grown in a buffer solution containing 50 mM imidazole, pH 7.5, 14–23% PEG3400, and 350 mM sodium acetate. Diffraction data were collected on the crystals at 100 K using the beamline 5.0.3 at the Advanced Light Source, Lawrence Berkeley National Laboratory. All diffraction data were processed using HKL2000. The structure was solved by molecular replacement with a ternary complex structure (PDB ID 1BPY) as a search model. The model was built into the electron density using COOT (37) and refined using PHENIX (38). MolProbity was used to make Ramachandran plots (39). All the crystallographic figures were generated using PyMOL.

Crystallization and structure determination of polη-DNA ternary complex

The template oligonucleotide for X-ray crystallographic studies of the ternary complex of polη (5′-CAT(oxoA)ATG ACGCT-3′) was synthesized by Midland Certified Reagent Co. (Midland, TX). The primer (5′-AGCGTCAT-3′) was synthesized by Integrated DNA Technologies (Coralville, IA, USA). The template and primer for polη structural studies were mixed at a 1:1 molar ratio and were annealed in HEN buffer (10 mM HEPES, pH 8.0, 0.1 mM EDTA and 50 mM NaCl) by heating for 10 min at 90°C and slow cooling to room temperature. The co-crystals of the ternary complex of polη-oxoA:dTTP* or polη-oxoA:dGTP* were grown at the similar conditions described previously (26). Briefly, freshly purified protein (∼8 mg/ml) and DNA were mixed at 1:1.5 molar ratio and diluted threefold by addition of 5 mM $MgCl_2$ in the gel filtration buffer. After being incubated on ice for 1 h, the complex was concentrated to the protein concentration of ∼3 mg/ml by ultrafiltration. Non-hydrolyzable nucleotides were added 10-fold molar excess to protein to form ternary complexes. All polη ternary complex crystals were grown by the hanging-drop vapor diffusion method. The optimized reservoir buffer contained 100 mM MES (pH 5.5), 5 mM $MgCl_2$, 16–21% (w/v) PEG 2K-MME. Extensive attempts for crystallizing Gln38Ala polη mutant incorporating dGTP* opposite templating oxoA were not successful. Diffraction data were collected at 100 K at the beamline 23-ID-D at the Advanced Photon Source, Argonne National Laboratory. All diffraction data were processed using HKL 2000. The structure was solved by molecular replacement with polη structure with an undamaged DNA (PDB ID 4O3N) as a search model (26).

Steady-state kinetics of single nucleotide incorporation opposite templating oxoA by wild-type polη and Gln38Ala polη

Steady-state kinetic parameters for insertion opposite oxoA by wild-type polη and Gln38Ala polη were measured with minor modification of protocols described previously (26).

All the oligonucleotides DNAs for kinetic assays were synthesized by Midland Certified Reagent Company (Midland, TX, USA) and Integrated DNA Technologies (Coralville, IA, USA). For the preparation of DNA substrate for polη-catalyzed incorporation, 34-mer template (5′-GTACCCG GGGATCCGTACG(X)CGCATCA GCTGCAG-3′ (X = oxoA, A, T) and 5′-FAM-labeled 14-mer primer (5′-FAM /CTGCAGCTGATGCG-3′) were annealed in a hybridization buffer (10 mM Tris–HCl pH 8.0, 1 mM EDTA). Enzyme activities were determined using the reaction mixture containing 40 mM Tris–HCl pH 8.0, 60 mM KCl, 10 mM dithiothreitol, 250 μg/ml bovine serum albumin, 2.5% glycerol, 5 mM $MgCl_2$, 100 nM primer/template DNA and varying concentration of incoming dTTP or dGTP. The insertion reactions were initiated by the addition of polη (2 nM) at 22°C. After 2 min, the reactions were stopped by adding 20 μl of a gel-loading buffer (95% formamide with 20 mM EDTA, 45 mM Tris-borate, 0.1% bromophenol blue, 0.1% xylene cyanol). The quenched reaction mixtures were separated by 20% polyacrylamide gel electrophoresis and analyzed as described above. To prevent end-product inhibition and substrate depletion from interfere with accurate velocity measurement, the enzyme concentrations and reaction-time intervals were adjusted for every experiment (less than 20% insertion product formed). The product formation was quantified by analyzing gels using a Storm 860 Imager (Molecular Dynamics) and ImageQuant software. The k_{cat} and K_m were determined by fitting reaction rate over dNTP concentrations to the Michaelis–Menten equation. Each experiment was repeated three times to measure the average of the kinetic results. The catalytic efficiency of nucleotide insertion was calculated as k_{cat}/K_m. The relative frequency of dNTP incorporation opposite oxoA was determined as $f = (k_{cat}/K_m)_{[dN:oxoA]}/(k_{cat}/K_m)_{[dT:dA]}$.

Steady-state kinetics of single nucleotide incorporation opposite templating oxoA by Asn279Ala mutant polβ

Steady-state kinetic parameters for insertion opposite oxoA by Asn279Ala mutant polβ were measured with minor modification of published protocols (21,40). Briefly, the oligonucleotides DNAs for kinetic assays (upstream primer, 5′-FAM/CTGCAGCTGATGCG-3′, downstream primer, 5′-phosphate/CGTACGGATCCC CGGGTAC-3′, and template, 5′-GTACCCGGGGATCCGTACG(oxoA) CGCATCAGCTGCAG-3′) were synthesized by Midland Certified Reagent Company (Midland, TX) and Integrated DNA Technologies (Coralville, IA, USA). To prepare DNA substrate containing a single-nucleotide gap opposite oxoA by Asn279Ala mutant polβ, the template, upstream primer, and downstream primer oligonucleotides were annealed in a hybridization buffer (10 mM Tris–HCl pH 7.5, 1 mM EDTA) by heating at 90°C for 5 min and slowly cooling down to room temperature. Enzyme activities were determined at 22°C by using the reaction mixture containing 50 mM Tris–HCl pH 7.5, 100 mM KCl, 5 mM $MgCl_2$, 1 mM dithiothreitol, 80 nM single-nucleotide gapped DNA, and varying concentration of incoming dTTP or dGTP. The catalytic efficiency of nucleotide insertion and the relative frequency of dNTP incorporation opposite oxoA were determined as described above.

RESULTS

Steady-state kinetics of nucleotide incorporation opposite dA or oxoA by Gln38Ala polη

Gln38 of polη plays a key role in replication across DNA lesions (41,42). To evaluate whether Gln38 contributes to the highly promutagenic bypass of oxoA by polη, we conducted steady-state kinetics for Gln38Ala polη incorporating dTTP or dGTP opposite dA or oxoA (Table 1 and Figure 2).

Kinetic studies showed the Gln38Ala mutation exhibited a differential impact on the insertion opposite dA and oxoA. During the bypass of templating dA, Gln38Ala polη mutant incorporated dTTP ∼1.5-fold (11.3×10^{-3} s^{-1} μM^{-1} versus 17.0×10^{-3} s^{-1} μM^{-1}) less efficiently than wild-type polη. The mutation increased K_m and k_{cat} ∼2.8-fold and ∼1.9-fold, respectively. For the incorporation of dGTP opposite dA, the mutation increased K_m and k_{cat} ∼3.0-fold and ∼1.7-fold, respectively, thereby decreasing the catalytic efficiency ∼1.7-fold. These results indicate that the presence of Gln38 does not significantly impact the efficiency of nucleotide insertion opposite an undamaged base. The wild-type and Gln38Ala polη displayed similar replication fidelity (inserting dTTP instead of dGTP), signifying that Gln38 does not significantly affect the fidelity for an undamaged base.

By contrast, the Gln38Ala mutation greatly affects the catalytic efficiency and replication fidelity for the bypass of the oxoA lesion. For correct dTTP insertion opposite oxoA, the Gln38Ala mutation lowered the catalytic efficiency by ∼4.3-fold (10.5 versus 2.4, Table 1). For the incorrect oxoA:dGTP insertion, the substitution dramatically reduced the efficiency by ∼55-fold. Specifically, K_m increased ∼23-fold (4.9 versus 113.8 μM), and k_{cat} decreased ∼2.4-fold (24.8×10^{-3} s^{-1} versus 10.5×10^{-3} s^{-1}). Previous studies have shown that wild type polη incorporates dGTP opposite oxoA with only ∼2-fold decrease in the efficiency (10.5×10^{-3} $s^{-1}\mu M^{-1}$ versus 5.1×10^{-3} $s^{-1}\mu M^{-1}$) relative to that for oxoA:dTTP insertion (21). When the Gln38Ala polη mutant was used, the efficiency dropped by ∼26-fold (2.4 versus 0.092). The mutation slightly increased K_m (∼1.6-fold, 71.3 versus 113.8 μM), whereas it reduced k_{cat} ∼17-fold (172.6×10^{-3} s^{-1} versus 10.5×10^{-3} s^{-1}), revealing that the Gln38Ala substitution made a greater impact on k_{cat}. During the bypass of oxoA, the polη mutant was ∼13-fold (27 versus 2) more accurate than wild-type polη, suggesting that Gln38 decreases the fidelity for the major oxidative adenine lesion. Overall, these kinetic results highlight Gln38 may significantly contribute to the polη-mediated promutagenic bypass of oxoA

Steady-state kinetics of nucleotide incorporation opposite dA or oxoA by Asn279Ala polβ

During correct insertion, Asn279 of polβ engages in a minor groove interaction with an incoming nucleotide (43). When bypassing dG, the mutation of Asn279 to alanine increases the catalytic efficiency and replication fidelity by ∼3-fold and ∼6-fold, respectively (44). To evaluate the impact of Asn279Ala mutation on the bypass of oxoA, we per-

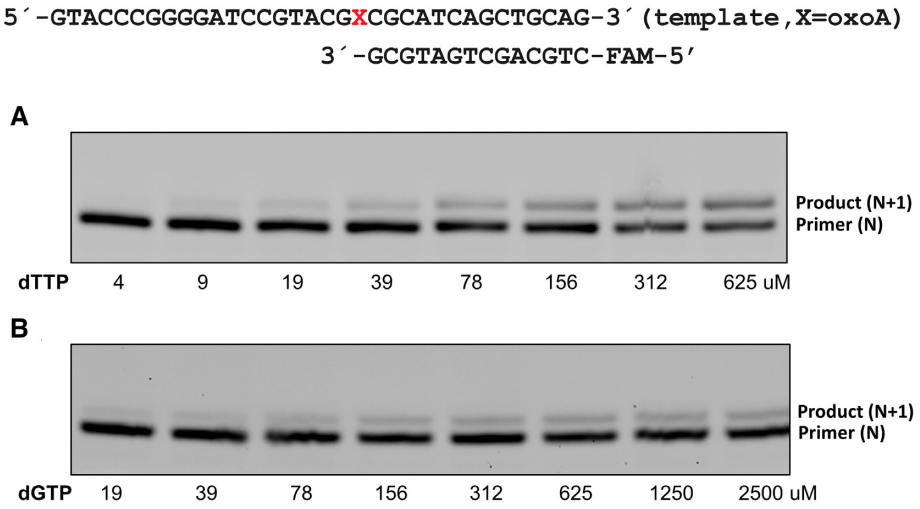

Figure 2. Representative denaturing PAGE gels for Gln38Ala polη mutant incorporating nucleotide opposite oxoA. Insertion of dTTP (**A**) or dGTP (**B**) opposite oxoA by Gln38Ala mutant polη. Annealed DNA of 5′-FAM-labeled primer and an oxoA-containing template were mixed with Gln38Al mutant polη, and the reactions were initiated by the addition of varying concentrations of dTTP or dGTP. All the reactions were conducted at 22°C, and the quenched samples were separated on 20% denaturing polyacrylamide gels.

Table 1. Kinetic parameters for nucleotide incorporation opposite oxoA by polη and Gln38Ala polη

template:dNTP	K_m (μM)	k_{cat} (10^{-3} s^{-1})	k_{cat}/K_m (10^{-3} s^{-1} μM^{-1})	f[a]	Replication fidelity
polη					
dA:dTTP[b]	5.4 ± 0.2	90.9 ± 5.8	17	1	200
dA:dGTP[b]	76.3 ± 4.8	6.3 ± 0.5	0.08	5×10^{-3}	
oxoA:dTTP[b]	3.6 ± 0.3	37.3 ± 2.3	11	6.2×10^{-1}	2
oxoA:dGTP[b]	4.9 ± 0.3	24.8 ± 1.3	5.1	3.0×10^{-1}	
dT:dGTP	74.3 ± 3.2	13.0 ± 0.2	0.18		
Q38A polη					
dA:dTTP	14.9 ± 1.3	167.3 ± 3.1	11.3	1	244
dA:dGTP	229.7 ± 11.6	10.5 ± 0.1	0.046	4.1×10^{-3}	
oxoA:dTTP	71.3 ± 4.4	172.6 ± 5.6	2.4	0.22	27
oxoA:dGTP	113.8 ± 2.8	10.5 ± 0.1	0.092	8.1×10^{-3}	

[a]Relative efficiency:$(k_{cat}/K_m)_{[dNTP:oxoA]}/(k_{cat}/K_m)_{[dTTP:dA]}$.
[b]Data from (21)

formed steady-state kinetic experiments of Asn279Ala polβ replicating opposite dA or oxoA (Table 2 and Figure 3).

The Asn279Ala mutation of polβ exhibited a differential impact on nucleotide insertion opposite dA and oxoA. The mutation decreased the catalytic efficiency for dA:dTTP insertion and dA:dGTP insertion by ∼2-fold and ∼4-fold, respectively, increasing the fidelity by ∼2-fold. While this substitution moderately decreased the efficiency for dA:dTTP insertion, it reduced the oxoA:dTTP insertion efficiency by ∼70-fold, revealing that Asn279Ala mutation exerts a greater impact on oxoA bypass. The reduction in the oxoA:dTTP insertion efficiency is primarily driven by an increased K_m. In addition, the mutation decreased the catalytic efficiency for oxoA:dGTP insertion ∼382-fold, dramatically deterring dGTP incorporation opposite the major oxidative adenine lesion. While the polη Gln38Ala mutation reduces the oxoA:dTTP-insertion efficiency 4-fold, the polβ Asn279Ala mutation reduces it 70-fold, highlighting the impact of the polymerase active site on an error-free bypass of oxoA. Overall, polβ kinetic studies demonstrate that Asn279 plays an important role in the promutagenic bypass of oxoA but not dA.

Structural basis for correct insertion opposite oxoA by polη

To gain structural insights into how TLS polymerases accurately replicate past the major oxidative adenine lesion, we determined a crystal structure of polη in complex with an incoming non-hydrolyzable dTMPNPP (dTTP* hereafter) paired with the templating oxoA. The non-hydrolyzable nucleotide analog was used for this crystallographic study because its coordination to the Mg^{2+} ion in the catalytic site is almost the same as that of normal nucleotide (45). The bridging N–H between P_α and P_β in the non-hydrolyzable nucleotide analog precludes nucleotidyl transfer, thereby enabling the use of a catalytically competent polymerase and physiologically relevant Mg^{2+} during crystallization studies. This also allows the primer terminus 3′-OH to coordinate with the catalytic metal ion. Non-hydrolyzable analogs have been successfully used for the structure de-

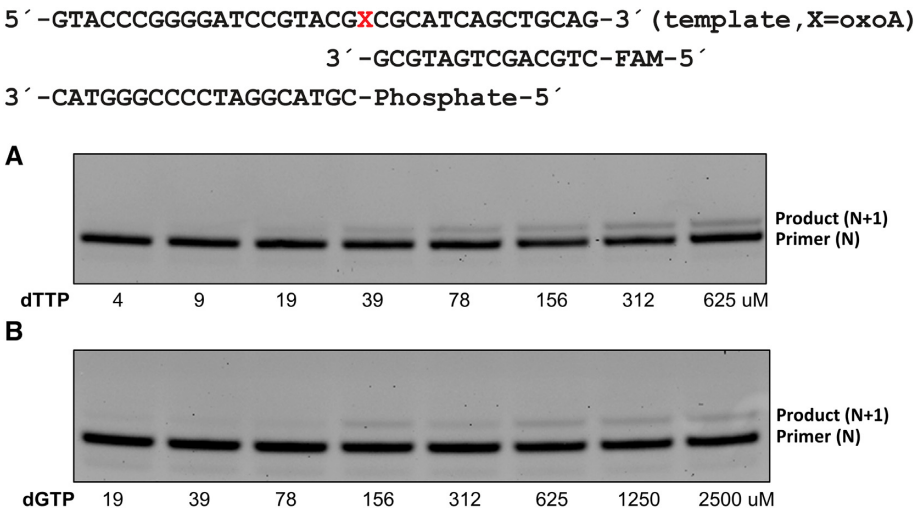

Figure 3. Denaturing PAGE gels for Asn279Ala polβ mutant incorporating nucleotide opposite oxoA. Single nucleotide incorporation of dTTP (panel **A**) or dGTP (panel **B**) opposite templating oxoA by the Asn279Ala polβ mutant. Annealed DNA of the 5′-FAM-labeled primer, downstream primer, and oxoA-containing template were mixed with the Asn279Ala polβ mutant, and the reactions were initiated by the addition of varying concentrations of dTTP or dGTP at 22°C. The quenched samples were separated on 20% denaturing polyacrylamide gels.

Table 2. Kinetic parameters for nucleotide incorporation opposite oxoA by wild-type and Asn279Ala polβ

template:dNTP	K_m (μM)	k_{cat} (10^{-3} s^{-1})	k_{cat}/K_m (10^{-3} s^{-1} μM^{-1})	f^a	Replication fidelity
polβ					
dA:dTTP[b]	0.9 ± 0.1	175.3 ± 4.7	200	1	
dA:dGTP[b]	107.4 ± 13.4	4.1 ± 0.3	0.039	1.9×10^{-4}	5287
oxoA:dTTP[b]	2.5 ± 0.2	193.6 ± 11.7	79	1	
oxoA:dGTP[b]	13.0 ± 0.8	84.2 ± 3.5	6.5	8.3×10^{-2}	12
N279A polβ					
dA:dTTP	1.9 ± 0.1	219.8 ± 3.8	120	1	
dA:dGTP	622.1 ± 17.6	5.6 ± 0.1	0.009	7.8×10^{-5}	12820
oxoA:dTTP	50.4 ± 6.3	56.2 ± 1.5	1.12	1	
oxoA:dGTP	316.1 ± 6.4	5.2 ± 0.3	0.017	1.5×10^{-2}	66

[a]Relative efficiency:$(k_{cat}/K_m)_{[dNTP:oxoA]}/(k_{cat}/K_m)_{[dTTP:dA]}$.
[b]Data from (44).

termination of various DNA polymerases (24,46). The polη-oxoA:dTTP* ternary complex structure was solved by molecular replacement and refined to 2.2 Å (Table 3).

The overall structure of the polη-oxoA:dTTP* complex was essentially identical to that of the polη-dG:dCTP* complex (PDB code 4O3N) (26); the root mean square deviation (RMSD) for these structures was 0.256 Å (Figure 4A). The polη-oxoA:dTTP* complex structure displayed the thumb, palm, finger and little finger domains of Y-family DNA polymerases. The templating oxoA was positioned between the finger and little finger domains, whereas the incoming dTTP* resided between the palm and finger domains.

The templating oxoA was in an *anti*-conformation and formed two Watson–Crick hydrogen bonds with the incoming dTTP* (Figure 4A). The active-site metal coordination in the polη-oxoA:dTTP* complex was virtually indistinguishable from that of the published polη-dG:dCTP* complex (Figure 4B). The primer terminus was coordinated to the A-site metal, 3.4 Å away from the Pα of incoming dTTP*, and well aligned for in-line nucleophilic attack on the Pα. The angle created by the primer terminus 3′-OH/Pα/bridging nitrogen was 171°, thereby placing the primer terminus 3′-OH in an optimal position for catalysis. Both A- and B-site metal ions were fully coordinated with ligands (e.g. Asp13, Met14, Asp115, Glu116, phosphate oxygens, water, primer terminus), showing that the polη-oxoA:dTTP* ternary complex was poised for nucleotidyl transfer reaction at the replication site. The templating oxoA and incoming dTTP* formed a coplanar base pair with interbase distances of 2.9 and 2.6 Å (Figure 4C). The base-pair geometry of oxoA:dTTP* was similar to that of the undamaged correct base pair (e.g., dG:dCTP): The C1′–C1′ distance was 10.2 Å and the λ angles were 58° and 62°, underscoring the presence of the 8-oxo moiety did not significantly alter base-pairing characteristics for correct insertion. OxoA in an *anti*-conformation was stabilized by stacking interactions with the templating dT at the N+1 position (Figure 4A). Gln38 from the finger domain was hydrogen bonded to the O4′ of the oxoA nucleotide and was 3.7 Å away from the N3 of oxoA (Figure 4D).

To evaluate whether oxoA in the replicating site alters the conformation of the protein and DNA, we compared

Table 3. Data collection and refinement statistics

PDB code	polη oxoA:T (6PL8)	polη oxoA:G (6PLC)	polβ N279A oxoA:G (6PKZ)
Data collection			
Space group	$P6_1$	$P6_1$	$P2_1$
Cell constants			
a (Å)	98.705	98.447	54.609
b	98.705	98.447	78.555
c	81.719	81.856	54.776
α (°)	90	90	90.00
β	90	90	106.83
γ	120	120	90.00
Resolution (Å)[a]	20–2.17 (2.21–2.17)	20–2.50 (2.54–2.50)	20–2.74 (2.79–2.74)
R_{merge}[b] (%)	0.141 (0.780)	0.147 (0.863)	0.126 (0.417)
$<I/\sigma>$	18.4 (2.55)	20.9 (2.68)	13.5 (2.31)
Completeness (%)	100.0 (100.0)	100.0 (100.0)	97.4 (95.1)
Redundancy	11.0 (10.0)	11.1(10.7)	3.9 (3.5)
Refinement			
R_{work}[c]/R_{free}[d] (%)	18.2/24.4	17.3/25.7	17.5/24.9
Unique reflections	24030	15731	11337
Mean *B* factor (Å^2)			
Protein	31.11	39.79	34.80
Ligand	30.89	36.33	42.20
Solvent	33.40	35.45	26.88
Ramachandran plot			
Most favored (%)	96.7	96.0	96.0
Add. allowed (%)	3.1	3.8	3.7
RMSD			
Bond lengths (Å)	0.009	0.010	0.011
Bond angles (°)	0.98	1.08	1.270

[a]Values in parentheses are for the highest resolution shell.
[b]$R_{merge} = \Sigma|I - \langle I \rangle| / \Sigma I$, where *I* is the integrated intensity of a given reflection.
[c]$R_{work} = \Sigma||F(obs) - F(calc)|| / \Sigma F(obs)$.
[d]$R_{free} = \Sigma||F(obs) - F(calc)|| / \Sigma F(obs)$, calculated using 5% of the data.

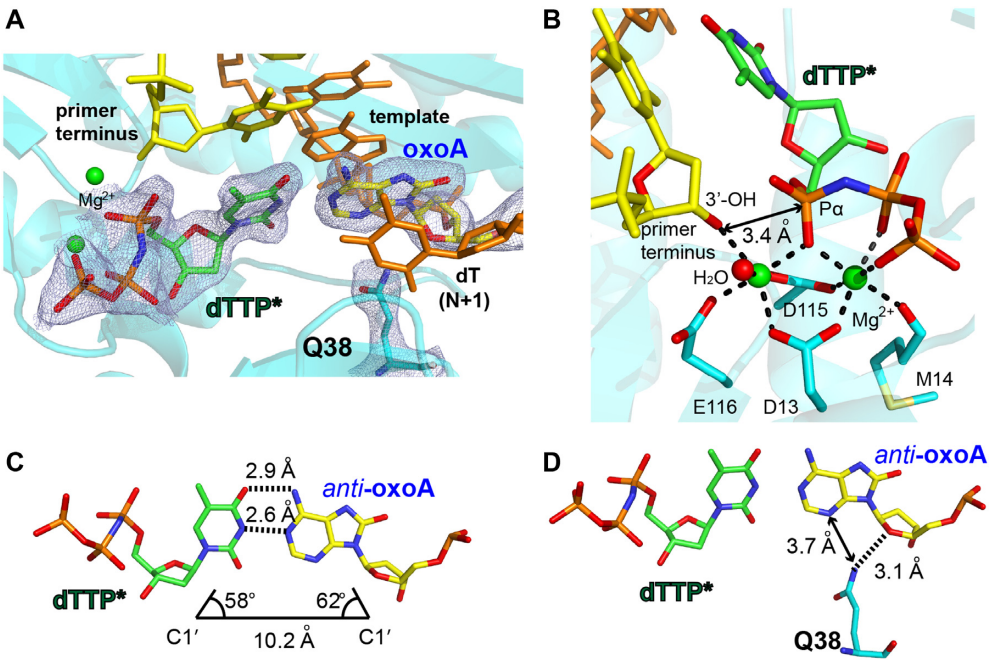

Figure 4. Structure of polη incorporating dTTP opposite the templating oxoA. (**A**) Close-up view of the catalytic site of the polη-oxoA:dTTP* structure. A $2F_o - F_c$ electron density map contoured at 1σ around oxoA:dTTP* is shown. OxoA and dTTP* are shown in yellow and green carbons, respectively. The catalytic Mg^{2+} ions are shown in green spheres. (**B**) Coordination of the active-site Mg^{2+} ions. (**C**) Watson–Crick base pairing of oxoA and dTTP* in the replicating site. OxoA is in an *anti*-conformation and forms two hydrogen bonds with the incoming dTTP*. Base pair geometry for oxoA:dTTP* is shown. (**D**) Hydrogen bonding interaction between Gln38 and templating oxoA.

the polη-oxoA:dTTP* structure with the published polη-dG:dCTP* structure (PDB code 4O3N) (26). The comparison revealed the protein conformations were very similar, whereas the DNA conformations near the templating bases in the N and N+1 positions were somewhat distinctive (Figure 5). In the polη-oxoA:dTTP* structure, the Arg61-Trp64 loop, which shifts in the presence of a bulky lesion (e.g. cisplatin-GpG, oxaliplatin-GpG, cyclobutane pyrimidine dimer (22,24,47)), did not undergo a conformational reorganization, suggesting the polη active site tolerated the major oxidative adenine lesion well. The oxidized purine oxoA at the templating position gave rise to a conformational adjustment of the 5′ phosphodiester and the DNA upstream of the lesion (Figure 5A). The base-pair geometry of oxoA:dTTP* was virtually identical to that of dG:dCTP* (Figure 5A). The 5′-phosphodiester of oxoA, however, moved away from the lesion, preventing steric and repulsive electrostatic interactions with the 8-oxo moiety (Figure 5B and C). In addition, the templating dT at the N+1 position in the oxoA:dTTP* structure moved toward the major groove relative to the dG:dCTP* structure, promoting stacking interaction with oxoA (Figure 5A). Overall, the conformational similarity of the oxoA:dTTP* and the dG:dCTP* structures is consistent with facile incorporation of dTTP opposite oxoA by polη.

Structural basis for incorrect insertion opposite oxoA by polη

Polη has been shown to incorporate dGTP opposite oxoA proficiently and extend past the oxoA:dG base pair efficiently (21). To gain structural insights into the mutagenic replication across oxoA, we determined a crystal structure of polη incorporating a non-hydrolyzable dGMPNPP (dGTP* hereafter) opposite oxoA. The polη-oxoA:dGTP* ternary complex was crystallized in the $P6_1$ space group, and this crystal contained one complex per asymmetric unit. The ternary structure was refined to 2.5 Å resolution. The overall structure of the polη-oxoA:dGTP* complex was similar to that of the polη-oxoA:dTTP* complex (RMSD = 0.302 Å).

The active-site metal ion coordination in the polη-oxoA:dGTP* structure was essentially identical to that observed in the correct insertion structures (Figure 6B). The A-site and B-site Mg^{2+} ions were chelated with the primer terminus 3′-OH, the catalytic triad (Asp13, Asp115 and Glu116 in the palm domain), the backbone carbonyl oxygen of Met14, three non-bridging phosphate oxygens of dGTP, and water, as observed in the polη-oxoA:dTTP* structure. The primer end 3′-OH was 3.2 Å away from the Pα of dGTP* and poised for in-line nucleophilic attack on the Pα.

The base pair conformation of oxoA:dGTP* in the polη active site was very different from that in the polβ active site, where oxoA and dGTP* adopt a Watson–Crick-like base-pair conformation with three interbase hydrogen bonds (Figure 1D). In the polη active site, oxoA and dGTP* were in a coplanar conformation and formed a wobble base pair with two interbase hydrogen bonds (Figure 6A and C). OxoA was in a *syn*-conformation and engaged in Hoogsteen pairing with dGTP* in an *anti*-conformation. The N7-H and O8 of *syn*-oxoA were hydrogen bonded to the O6 (3.2 Å) and N1-H (2.8 Å) of *anti*-dGTP*, respectively. The oxoA:dGTP base pair formed a wobble geometry: The λ angles for oxoA:dGTP* were 68° and 45°, respectively.

The wobble oxoA:dGTP* conformation in the polη active site was stabilized by a Gln38-mediated minor groove contact. In the polη-oxoA:dGTP* structure, the minor groove interaction between Gln38 and the nascent base pair, which was lacking in the corresponding oxoA:dTTP* structure, was present. It has been shown that Gln38 from the finger domain typically engages in minor groove interactions with a templating base in the accurate bypass of an undamaged base (26,41,48). In the polη-oxoA:dGTP* structure, Gln38 made hydrogen bond contacts to the minor groove edge of the incoming dGTP* and possibly *syn*-oxoA (Figure 6D), which could stabilize the wobble oxoA:dGTP* base-pair conformation in the nascent base pair site of polη. Specifically, the side chain amide NH_2 of Gln38 was 3.5 Å away from the O8 of the templating oxoA, suggesting the formation of a weak hydrogen bonding. In addition, the side chain carbonyl oxygen of Gln38 was 3.3 Å away from the N2 of dGTP*, indicating the formation of a hydrogen bond between the incoming nucleotide and Gln38. These minor groove recognition contacts by Gln38 would stabilize a wobble conformation of oxoA:dGTP* in the replication site, resulting in a lower K_m for the oxoA:dGTP insertion compared to the dA:dGTP insertion (4.87 versus 76.29 μM, Table 1). The removal of the minor groove interaction via Gln38Ala mutation resulted in a ∼55-fold reduction in the catalytic efficiency (5.1 versus 0.092), which was primarily driven by an increased K_m (4.87 versus 113.8, Table 1). This underscores that Gln38-mediated minor groove contacts promotes the promutagenic incorporation of dGTP opposite oxoA.

Protein and template DNA adjusted their conformations to accommodate a wobble *syn*-oxoA:*anti*-dGTP base pair in the polη catalytic site (Figure 7). Overlay of the polη-oxoA:dGTP* structure with the published polη-dG:dCTP* structure (PDB code 4O3N) (26) showed that the templating dT at the N+1 position of the oxoA:dGTP* structure shifted 5–6 Å away from Gln38 compared with the oxoA:dTTP* and the dG:dCTP* structures (Figure 7A and B), which allowed stacking with the 6-membered ring of *syn*-oxoA. Another conformational difference was observed with the loop containing Gln38 (Figure 7C). Compared with the oxoA:dTTP* and dG:dCTP* structures, the side chain of Gln38 in the oxoA:dGTP* complex moved toward the replicating base pair by 1.5 and 1.1 Å, respectively (Figure 7C). This movement, which has been rarely observed in published polη structures, permitted Gln38 to engage in the minor groove interactions with the incoming nucleotide and perhaps the templating base.

The Gln38-mediated minor groove interaction with the incoming nucleotide is present in the oxoA:dGTP* structure but not in the published polη-oxoG:dATP* structure (PDB code 4O3O) (26) (Figure 8A and B), suggesting a differential effect of Gln38 in the mutagenic bypass of the major oxidative purine. Superposition of the polη-oxoA:dGTP* and polη-oxoG:dATP* structures reveals that the side-chain amide of Gln38 interacts with an incoming nucleotide in the oxoA:dGTP* structure,

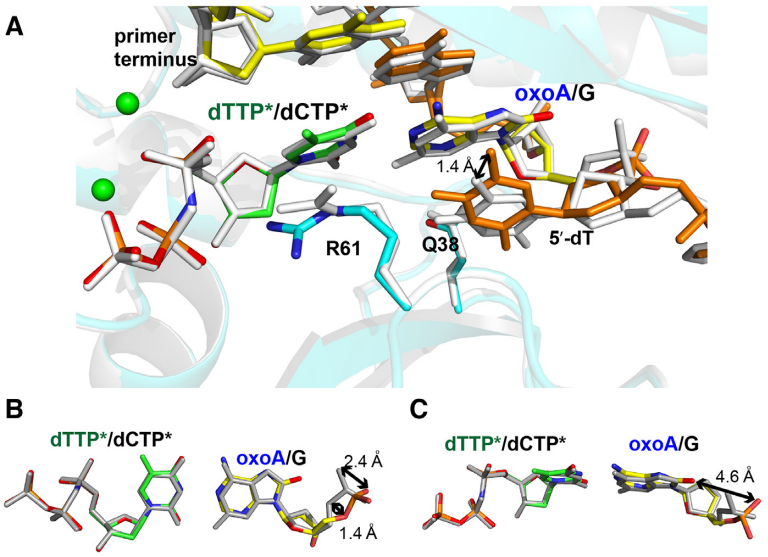

Figure 5. Comparison of the polη-oxoA:dTTP* structure with published polη-dG:dCTP* structure. (**A**) Close-up view of the nascent base pair binding site of the complexes. The color scheme for the polη-oxoA:dTTP* is the same as in Figure 3B. The polη-dG:dCTP* structure (PDB code 4O3N) is colored in white. (**B**) Superposition of the oxoA:dTTP* and dG:dCTP* base pairs. Distances are indicated as double-headed arrows. (**C**) Side view of the oxoA:dTTP* and dG:dCTP* base pairs. Distance between the O8 of oxoA and the non-bridging oxygen of the 5′-phosphate oxygen is indicated.

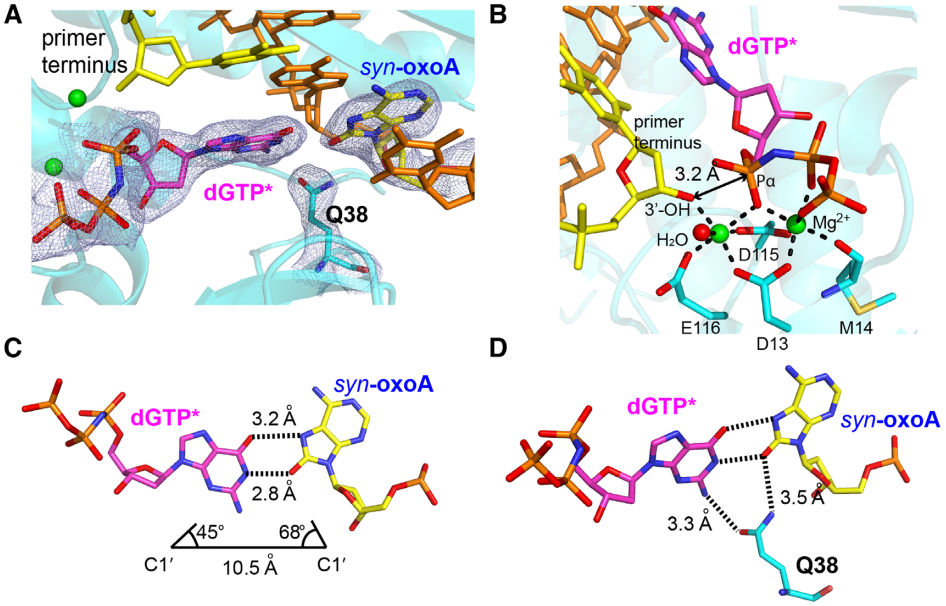

Figure 6. Structure of polη incorporating dGTP opposite templating oxoA. (**A**) Close-up view of the catalytic site of the polη-oxoA:dGTP* complex. OxoA and dGTP* are colored in blue and magenta, respectively. A $2F_o - F_c$ electron density map contoured at 1σ around oxoA:dGTP* is shown. OxoA is in *syn*-conformation and forms a coplanar base pairing with dGTP*. (**B**) Coordination of the active site metal ions with primer terminus 3′-OH, dGTP*, the catalytic carboxylates, and Met14. The distance between the primer terminus 3′-OH and Pα is indicated. (**C**) Base pairing properties of oxoA and dGTP* with a wobble configuration. The C1′-C1′ distance for oxoA:dGTP* and the λ angles are shown. (**D**) Minor groove interaction of a wobble oxoA:dGTP* base pair with Gln38 of polη. Distances between the amide moiety of Gln38 and the N2 of dGTP* or the O8 of oxoA are indicated.

while it is hydrogen-bonded only to the templating oxoG in the oxoG:dATP* structure (Figure 8C). Gln38 in the oxoA:dGTP* structure shifts toward the minor groove edge by ∼0.7 Å relative to the position in the oxoG:dATP* structure. The conformation of oxoA:G with a wobble geometry markedly deviates from that of oxoG:A with a Watson–Crick-like geometry (Figure 8B and D). OxoA moves toward the major groove by 1.4–2.1 Å relative to oxoG, whereas dGTP* moves toward the minor groove by ∼1.6 Å relative to dATP* (Figure 8D). The nucleobase of the 5′-dT ($N + 1$) in the oxoA:dGTP* structure shifts ∼4 Å and rotates 45° clockwise away from Gln38 relative to the position in the oxoG:dATP* structure, thereby making stacking interactions with the 6-membered ring of oxoA. This rotation

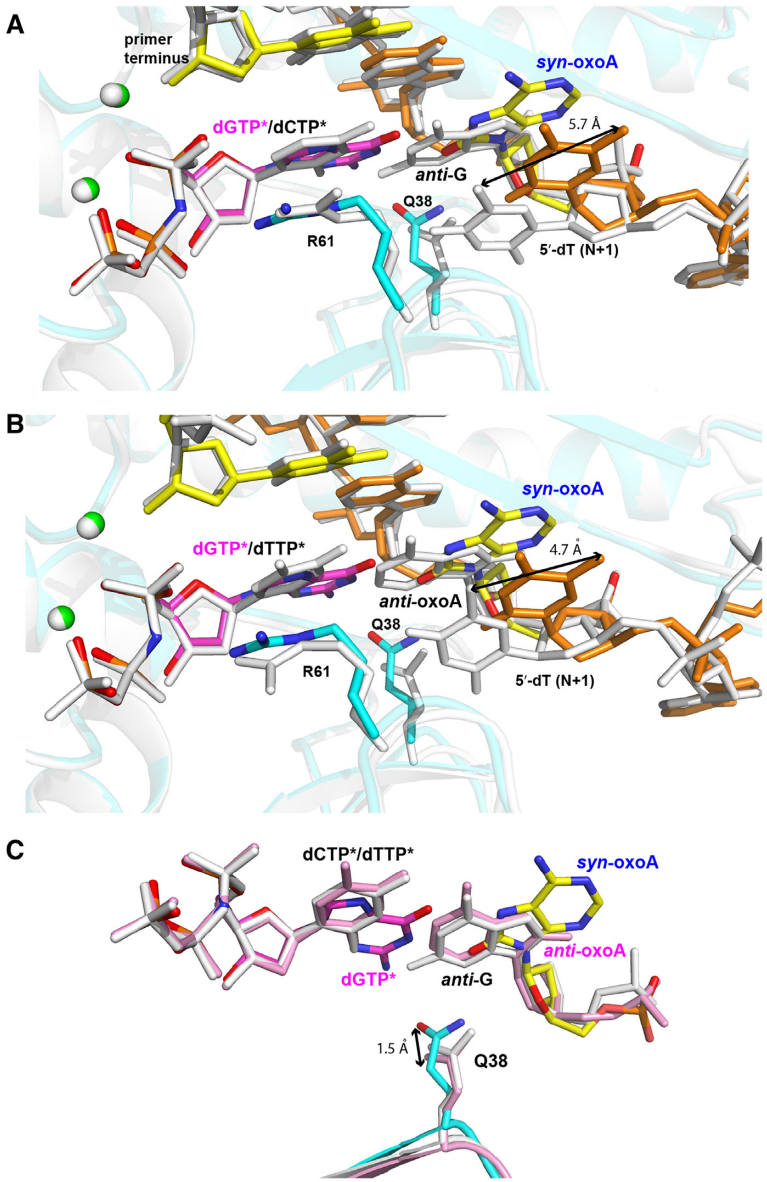

Figure 7. Comparison of conformations of oxoA:dGTP*, oxoA:dTTP* and dG:dCTP* base pairs in polη active site. (**A**) Superposition of the polη-oxoA:dGTP* structure and published polη-dG:dCTP* (PDB ID 3O3N) structure in the catalytic site. (**B**) Superposition of the polη-oxoA:dGTP* and polη-oxoA:dTTP* structures in the catalytic site. (**C**) Conformational difference of Gln38 in the polη-oxoA:dGTP*, polη-dG:dCTP* and polη-oxoA:dTTP* structures. The distance between the amide oxygens in the oxoA:dGTP* and the dG:dCTP* structures is indicated.

occurs with minimal perturbation at the sugar moiety of the 5′-dT (N+1). Previous studies show that the Gln38Ala mutation decreases oxoG:dATP insertion efficiency only 4-fold (41), which is much lower than the 55-fold reduction for the oxoA:dGTP insertion efficiency.

Overall, this structure reveals the structural basis for the efficient incorporation of dGTP opposite oxoA by TLS polη. The observation of a wobble oxoA:dGTP base-pair conformation stabilized by Gln38-mediated minor groove contacts as well as the large reduction in catalytic efficiency via the Gln38Ala mutation highlight that the GLn38-mediated minor groove interaction in the nascent base pair site facilitates the proficient and mutagenic bypass of oxoA by polη.

Structure of Asn279Ala polβ incorporating dGTP* opposite oxoA

While oxoA:dGTP* adopts a wobble conformation in the wild-type polη active site, it takes on Watson–Crick-like conformation in the wild-type polβ active site, highlighting the influence of polymerase microenvironment on the base pair conformation of oxoA:dGTP. In the polβ structure with Watson–Crick or Watson–Crick-like nascent base pair conformation (21), Asn279 and Arg283 make minor groove recognition contacts to the incoming nucleotide and templating base, respectively. We wanted to evaluate the possibility that the minor groove interaction between Asn279 of polβ and N3 of dGTP facilitates the formation of the oxoA:dGTP with Watson–Crick-like geometry

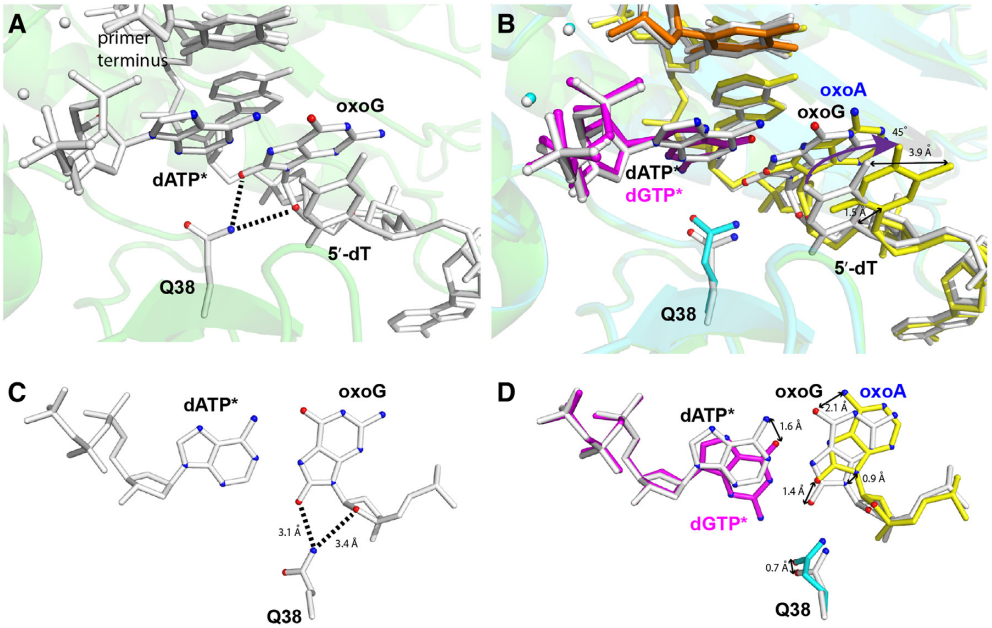

Figure 8. Conformations of oxoA:dGTP* and oxoG:dATP* base pairs in polη catalytic site. (**A**) Close-up view of the active site of published polη-oxoG:dATP* structure (PDB code: 4O3O). Gln38-mediated hydrogen bonds to *syn*-oxoG are indicated as dotted lines. (**B**) Superposition of oxoA:dGTP* (multiple colors) and oxoG:dATP* (gray) base pairs in polη active site. Distances are indicated as double-headed arrows. (**C**) Minor groove interaction between oxoG and Gln38 in the published polη-oxoG:dATP* structure. (**D**) Superposition of oxoA:dGTP* (multiple colors) and oxoG:dATP* (white) base pairs. Distances are indicated as double-headed arrows.

by promoting ionization or enol tautomerization of dGTP (Figure 1D). Our kinetic studies showed a ∼380-fold reduction in the efficiency for the oxoA:dGTP insertion in the presence of an Asn279Ala mutation (Table 2), suggesting that Asn279 may play a role in the promutagenic bypass of oxoA. This is in stark contrast with published reports that the Asn279Ala substitution only moderately alters the catalytic efficiency for correct insertion (44). To gain insights into the role of Asn279 in oxoA bypass, we determined a crystal structure of Asn279Ala polβ in complex with oxoA:dGTP*, which was refined to 2.7 Å resolution (Table 3). The Asn279Ala polβ-oxoA:dGTP* ternary complex was crystallized in the $P2_1$ space group, which has also been observed for the wild-type polβ-oxoA:dGTP* complex.

The Asn279Ala polβ-oxoA:dGTP* structure was very different from the wild type polβ-oxoA:dGTP* structure (RMSD = 1.310 Å), illustrating that the minor groove interaction between Asn279 and incoming dGTP greatly affected the oxoA:dGTP base pair conformation (Figure 9A). In the published wild-type polβ-oxoA:dGTP* structure (PDB code 6E3W), polβ is in a closed conformation, where the α-helix N and the primer terminus base-pair sandwich the nascent oxoA:dGTP*. In the wild-type polβ active site, oxoA:dGTP* assumes a coplanar base-pair conformation with Watson–Crick-like geometry, where *syn*-oxoA and *anti*-dGTP* form three interbase hydrogen bonds. In contrast, our mutant polβ was in an open conformation, where the α-helix N did not undergo an open-to-closed conformational reorganization. In addition, the nascent oxoA:dGTP* base-pair adopted a buckled conformation rather than a coplanar conformation (Figure 9A). Interestingly, both oxoA and dGTP* were in a *syn* conformation. Instead of forming three interbase hydrogen bonds, the O6 of the incoming *anti*-dGTP* formed bifurcated hydrogen bonds with N6 and N7-H of the templating oxoA (Figure 9B). Tyr271, which engages in a minor groove interaction with the primer terminus in correct insertion structure, was hydrogen bonded to O8 of oxoA, stabilizing the *syn*-oxoA conformation at the templating position (Figure 9A). The templating oxoA shifted toward the incoming dGTP* by ∼2.1 Å and the *syn*-dGTP* moved ∼2.4 Å away from the active site relative to the position observed in the wild type polβ-oxoA:dGTP* structure (Figure 9C), which resulted in the formation of a buckled oxoA:dGTP* conformation (∼130°). In the mutant structure, the critical catalytic A-site metal ion was absent. Only the B-site metal ion, or the nucleotide-binding metal ion, was coordinated to ligands, including Asp190, Asp192, H_2O, and dGTP phosphate oxygens (Figure 9A). While the nucleotide-binding metal ion is apparently present, it is not positioned in the B-site because polβ is in an open protein conformation.

While Arg283 plays a crucial role in stabilizing a closed conformation, Asn279 does not appear to be essential for the formation of a crystal with a closed conformation; the published Asn279Ala polβ-dG:dCTP* structure shows a closed protein conformation and Watson–Crick dG:dCTP* base pair (PDB ID 4Z6C) (44). Therefore, the open protein conformation observed in the Asn279Ala polβ-oxoA:dGTP* structure is likely to be induced by the formation of a non-Watson–Crick-like oxoA:dGTP* base pair. The non-Watson–Crick-like oxoA:dGTP can be dis-

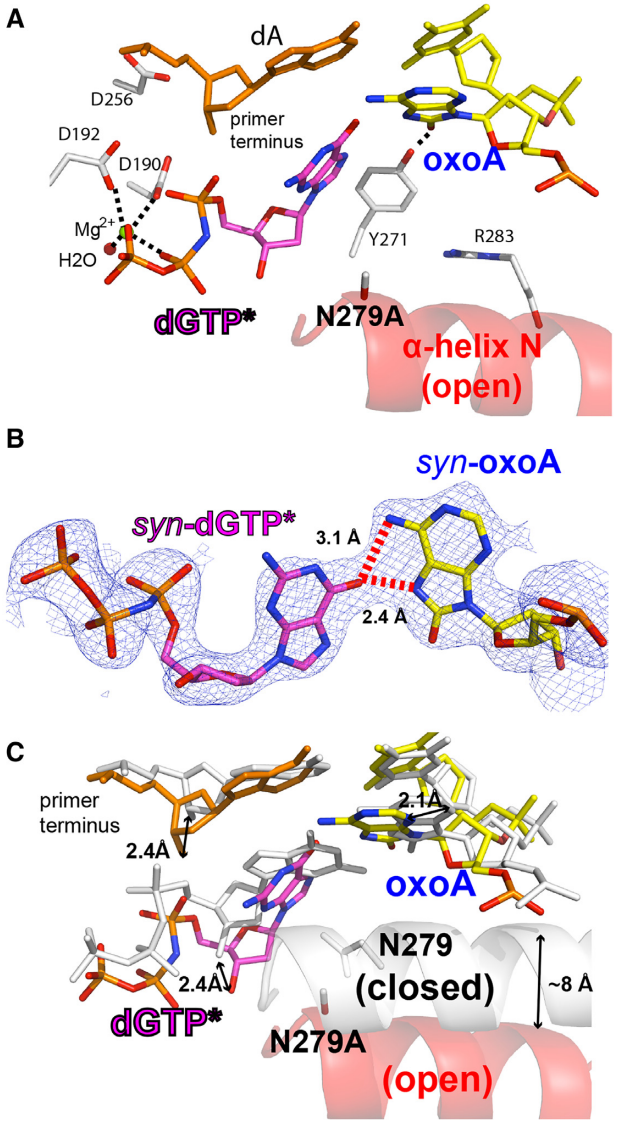

Figure 9. Structure of Asn279Ala polβ in complex with templating oxoA paired with an incoming dGTP*. (**A**) Close-up view of the catalytic site of the Asn279Ala polβ-oxoA:dGTP* structure. The α-helix N is in an open conformation. Mg^{2+} ion is shown in a green sphere. Protein is in an open conformation and oxoA:dGTP* adopts a buckled conformation. (**B**) Base pairing between *syn*-oxoA and *syn*-dGTP*. A $2F_o - F_c$ electron density map contoured at 1σ around oxoA:dGTP* is shown. Bifurcated hydrogen bonds are indicated as dotted lines. (**C**) Superposition of the Asn279Ala polβ-oxoA:dGTP* structure with the published wild-type polβ-oxoA:dGTP* structure (PDB ID 6E3W).

criminated by the protein that displays a stringent geometric selection mechanism. Taken together, the conformational differences observed between the wild type and mutant polβ-oxoA:dGTP* structures suggest that the minor groove contact of Asn279 to dGTP is critical for the formation of Hoogsteen oxoA:dGTP with Watson–Crick-like geometry. The Asn279Ala polβ-dG:dCTP* structure with an open protein conformation, a buckled oxoA:dGTP* conformation and one metal ion explains the drastic reduction in the efficiency for oxoA:dGTP insertion by the mutant protein.

DISCUSSION

Role of polη Gln38 in promutagenic bypass of oxidized purines

The minor groove recognition amino acid residue Gln38 of polη appears to modulate the efficiency and fidelity in a templating base-dependent manner. For correct insertion, Gln38 typically engages in hydrogen bonding interactions with the minor groove edge and O4′ of a templating base (26,41). For bypass of a templating dA, the Gln38Ala mutation does not significantly decrease the efficiency for neither dTTP nor dGTP insertion and thus only slightly changes the fidelity. In the presence of a templating dG, the mutation decreases dCTP insertion efficiency ∼4-fold and increases dATP insertion efficiency ∼2-fold (41), thereby reducing the fidelity by 8-fold. When oxoG is at the templating position, Gln38Ala substitution reduces the efficiency for dCTP (correct insertion) and dATP (misinsertion) by ∼3-fold and ∼4-fold, respectively, negligibly altering the fidelity (41). This indicates that the minor groove interaction between Gln38 and O8 of *syn*-oxoG or N3 of *anti*-oxoG exhibit a similar impact on the efficiency and fidelity. In the presence of templating oxoA, the same substitution lowers the catalytic efficiency for dTTP (correct insertion) and dGTP (misinsertion) by ∼4-fold and ∼55-fold, respectively, thereby reducing the fidelity by ∼13-fold. This underscores the greater impact of Gln38 on misinsertion during oxoA bypass. The differential impact of the Gln38Ala mutation on the efficiency and fidelity may result from the difference in minor groove interactions in the replication site. Hydrogen bond interactions between Gln38 and an incoming nucleotide, which is found in the oxoA:dGTP base pair, may greatly decrease K_m and thus promote a mutagenic bypass. The abrogation of the Gln38–dGTP interaction leads to a drastic reduction in misincorporation efficiency for oxoA:dGTP.

While the abolition of Gln38-mediated minor groove interactions only slightly decreases the fidelity for oxoG bypass, it increases the fidelity of oxoA bypass by 13-fold, indicating that Gln38 significantly promotes mutagenic bypass of the major oxidative adenine lesion but not the major oxidative guanine lesion. This difference may be related to the conformational differences in oxoA:dGTP and oxoG:dATP in the polη active site. While oxoG:dATP adopts a Watson–Crick-like conformation in the absence of minor groove protein contacts, oxoA:dGTP forms a wobble configuration that is stabilized by the Gln38-mediated contact. In the case of oxoG, Gln38 interacts with the minor groove edge of the templating base in both oxoG:dATP and oxoG:dCTP base pairs. In the case of oxoA, Gln38 interacts with the templating base for oxoA:dTTP and the minor groove edge of the incoming nucleotide for oxoA:dGTP. Overall, Gln38 of polη displays a differential impact on the mutagenic bypass of oxoA and oxoG.

Role of polη Arg61 in the discrimination of a wobble mismatch in polη active site

DNA polymerases employ varying degrees of geometric constraints to increase the replication fidelity (49–51). In most polymerase active sites, Watson–Crick or Watson–Crick-like base pair conformations are preferentially ac-

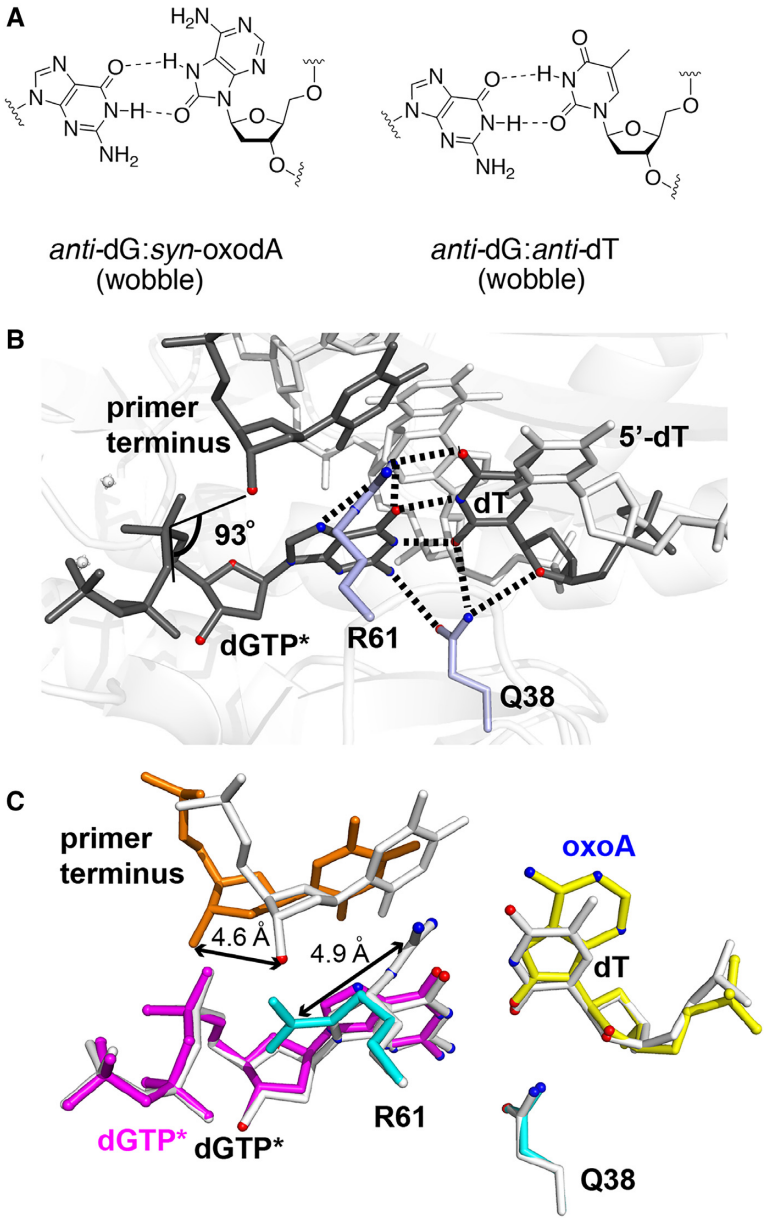

Figure 10. Comparison of dT:dGTP* and oxoA:dGTP* base pairs in polη active site. (**A**) OxoA:G and T:G base pair with wobble geometry. (**B**) Close-up view of the catalytic site of published polη-dT:dGTP* structure (PDB code 4J9K). Hydrogen bonds by Arg61 and Gln38 are indicated. Primer terminus, dGTP*, and the templating dT is shown in gray. Arg61 and Gln38 are shown in light blue. (**C**) Overlay of primer terminus, incoming nucleotide, templating base, Arg61 and Gln38 in the polη-dT:dGTP* (4J9K, multiple colors) and polη-oxoA:dGTP* (white) structures.

commodated over the wobble base pair conformation. For example, oxoG causes G-to-T transversions by its ability to escape the geometric discrimination through formation of oxoG:A with Watson–Crick-like geometry, which is readily tolerated in the polymerase active site. The efficient incorporation of dGTP opposite oxoA by polη is thus quite unexpected because oxoA:dGTP assumes a wobble base pair conformation, the formation of which is typically deterred in the polymerase active site. While both dT:dGTP and oxoA:dGTP base pairs take on a wobble conformation in the polη active site (Figure 10A), dT:dGTP insertion is much less efficient than the oxoA:dGTP insertion (52). Particularly, the efficiency for oxoA:dGTP insertion is one half of that for oxoA:dTTP insertion and one third of that for dA:dTTP insertion. By contrast, the efficiency for dT:dGTP insertion reduced ∼40-fold to 320-fold compared with correct insertion (dT:dATP) in a sequence-dependent manner (52). Our kinetic studies show the dT:dGTP insertion is ∼28-fold less efficient than the oxoA:dGTP insertion (Table 1). These suggest the polη active site is better equipped to discriminate a wobble dT:dGTP than a wobble oxoA:dGTP.

How does the polη active site deter dT:dGTP insertion while it frequently allows oxoA:dGTP insertion? Comparison of the polη-oxoA:dGTP* structure with published polη-dT:dGTP* structure (PDB ID 4J9K) (52) sheds light

on the impact of the polymerase active site on mutagenic replication. The large difference in the misincorporation efficiency may result from the difference in the orientation of the primer terminus, which appears to be triggered by Arg61 (Figure 10). In the catalytic site of polη, both oxoA:dGTP and dT:dGTP take on a wobble conformation, and their minor groove edges are contacted by Gln38 (Figure 10B). A noteworthy conformational deviation is, however, observed in Arg61, which is known to play a role in lesion bypass (41,42,53). While Arg61 engages in major groove contacts with the dT:dGTP base pair, it interacts with the phosphate oxygen of the incoming nucleotide in the oxoA:dGTP base pair, as typically observed in correct insertion (Figure 10C). This conformational difference could be caused by the differential interaction of Arg61 with the major groove edge of the base pairs. Specifically, while dT:dGTP contains three hydrogen bond acceptors (N7 and O6 of dGTP and O4 of dT) in the major groove, oxoA:dGTP has three hydrogen bond acceptors and a hydrogen bond donor (N7 and O6 of dGTP and N6 and N1 of oxoA). In the dT:dGTP structure, the guanidium moiety of Arg61 donates three hydrogen bonds to make extensive major groove contacts to the nascent base pair, which would greatly stabilize the wobble dT:dGTP base-pair conformation. To accommodate this unusual Arg61 conformation, the primer terminus shifts toward the templating base, leading to the stacking interaction with Arg61. Consequently, the primer terminus 3′-OH is poorly aligned for in-line nucleophilic attack on the Pα of dGTP (Figure 10B, angle of 93°). Therefore, for the nucleotidyl transfer to occur, the primer terminus must undergo a conformational change. By contrast, in the oxoA:dGTP* structure, the primer terminus 3′-OH is nearly ideally (angle of 164°) positioned for catalysis and thus does not require significant conformational adjustment, which is consistent with the facile incorporation of dGTP opposite oxoA. As Arg61 is incapable of making extensive major groove contacts with *syn*-oxoA, Arg61-mediated major groove interactions in the oxoA:dGTP* complex would be less favorable than that in the dT:dGTP* complex, which would steer Arg61 to interact with the phosphate oxygen. In the nascent base pair site, Arg61 of polη would deter the dT:dGTP insertion but not the oxoA:dGTP insertion.

Impact of polβ Asn279-mediated minor groove contact on replication

DNA polymerase minor groove contacts have been shown to modulate mutagenic replication (44,54–58). The X-family polβ engages in minor groove interactions with the templating base and incoming nucleotide by using Arg283 and Asn279, respectively. During error-prone bypass of oxoG, Arg283 of polβ makes minor groove contact to O8 of *syn*-oxoG at the templating position (6), which in turn stabilizes the Hoogsteen *syn*-oxoG:*anti*-dATP base pair at the replication site. The abrogation of the Arg283-mediated minor groove interaction induces *anti*-oxoG conformation and an open protein conformation (58). Asn279 of polβ interacts with the minor groove edge of an incoming nucleotide during correct insertion. Asn279Ala substitution modestly changes the catalytic efficiency for the bypass of an undamaged base (44). For example, for the bypass of dG, the mutation increases the efficiency and fidelity 3-fold and 6-fold, respectively. For bypass of dA, Asn279Ala mutation decreases the efficiency by 2-fold and increases the fidelity by 2-fold. In contrast, when Asn279Ala polβ bypasses oxoA, the substitution reduces the efficiency for correct and incorrect insertion by ∼70-fold and ∼380-fold, respectively, highlighting a differential impact of Asn279 on the bypass of undamaged base and lesion. During bypass of the normal base, the Asn279-mediated minor groove contact is not required for the formation of a closed conformation, as seen in published Asn279Ala polβ-dG:dCTP* structure with a closed protein conformation (PDB ID 4Z6C). Asn279 is implicated in stabilizing *syn*-oxodGTP opposite dA (59), as the Asn279Ala mutation results in preferential incorporation of oxodGTP opposite dC. Minor groove recognition contact by Asn279 influences base pair conformation of certain mismatches. For instance, dG:dTTP, which can form a Watson–Crick-like conformation in the active site of wild-type polβ active site (60), takes on a wobble conformation in the presence of an Asn279Ala mutation (44). In addition, oxoA:dGTP, which is in a Watson–Crick-like conformation in the wild-type polβ active site, adopts a buckled conformation in the absence of Asn279-mediated contact.

CONCLUSIONS

In summary, the present studies further our understanding of the mutagenic potential and dual-coding characteristics of the major oxidative adenine lesion. The structural basis for the efficient promutagenic replication across oxoA by polη provides insight into oxoA-mediated mutagenesis in humans. While the polη active site deters dT:dGTP insertion, it promotes oxoA:dGTP insertion. OxoA:dGTP represents a rare example of a wobble mismatch that is proficiently catalyzed by DNA polymerases. The mutagenic bypass of oxoA by polη is greatly facilitated by Gln38-mediated minor groove contact to the incoming nucleotide, the abrogation of which dramatically reduces the catalytic efficiency and increases the replication fidelity. In addition, Arg61, which slows dT:dGTP insertion via unusual major groove contacts, interacts with the phosphate oxygen of dGTP opposite oxoA, thereby failing to discriminate oxoA:dGTP in the polymerase active site. In polβ's active site, the Asn279-mediated minor groove contact with dGTP appears to stimulate mutagenic replication across oxoA greatly and induce Watson–Crick-like oxoA:dGTP base-pair conformation. The present studies unveil a key difference in the mutagenesis mechanisms of oxoG and oxoA. While the mutagenicity of oxoG is mainly attributed to the lesion's flexibility, enabling favorable formation of oxoG:dA with a Watson–Crick-like geometry, the mutagenicity of oxoA in humans may be greatly induced by minor groove interactions.

DATA AVAILABILITY

PDB IDs: 6PL8, 6LPC and 6PKZ.

ACKNOWLEDGEMENTS

We are grateful to Dr Arthur Monzingo for technical assistance. Instrumentation and technical assistance for this

work were provided by the Macromolecular Crystallography Facility, with financial support from the College of Natural Sciences, the Office of the Executive Vice President and Provost, and the Institute for Cellular and Molecular Biology at the University of Texas at Austin. The Berkeley Center for Structural Biology is supported in part by the National Institute of General Medical Sciences of the National Institute of Health. The Advanced Light Source is supported by the Director, Office of Science, Office of Basic Energy Sciences, of the U.S. Department of Energy under Contract No. DE-AC02-05CH11231.
Author contributions: M.K. cloned, expressed and purified wild-type polη, performed wild-type polη crystallization, and wrote the manuscript; H.J. cloned, expressed, and purified Gln38Ala polη, performed mutant polη kinetics, and wrote the manuscript. S.L. managed the project, designed experiments and wrote the manuscript.

FUNDING

National Institutes of Health (NIH) [ES-26676] (in part). Funding for open access charge: NIH [ES-26676].
Conflict of interest statement. None declared.

REFERENCES

1. Talhaoui,I., Couvé,S., Ishchenko,A.A., Kunz,C., Schär,P. and Saparbaev,M. (2013) 7, 8-Dihydro-8-oxoadenine, a highly mutagenic adduct, is repaired by Escherichia coli and human mismatch-specific uracil/thymine-DNA glycosylases. *Nucleic Acids Res.*, **41**, 912–923.
2. Grollman,A.P. and Moriya,M. (1993) Mutagenesis by 8-oxoguanine: an enemy within. *Trends Genet.*, **9**, 246–249.
3. Hsu,G.W., Ober,M., Carell,T. and Beese,L.S. (2004) Error-prone replication of oxidatively damaged DNA by a high-fidelity DNA polymerase. *Nature*, **431**, 217–221.
4. Brieba,L.G., Eichman,B.F., Kokoska,R.J., Doublié,S., Kunkel,T.A. and Ellenberger,T. (2004) Structural basis for the dual coding potential of 8-oxoguanosine by a high-fidelity DNA polymerase. *EMBO J.*, **23**, 3452–3461.
5. Beard,W.A., Batra,V.K. and Wilson,S.H. (2010) DNA polymerase structure-based insight on the mutagenic properties of 8-oxoguanine. *Mutat. Res.*, **703**, 18–23.
6. Batra,V.K., Shock,D.D., Beard,W.A., McKenna,C.E. and Wilson,S.H. (2012) Binary complex crystal structure of DNA polymerase β reveals multiple conformations of the templating 8-oxoguanine lesion. *Proc. Natl. Acad. Sci. U.S.A.*, **109**, 113–118.
7. Jaruga,P. and Dizdaroglu,M. (1996) Repair of products of oxidative DNA base damage in human cells. *Nucleic Acids Res.*, **24**, 1389–1394.
8. Fuciarelli,A.F., Wegher,B.J., Gajewski,E., Dizdaroglu,M. and Blakely,W.F. (1989) Quantitative measurement of radiation-induced base products in DNA using gas chromatography-mass spectrometry. *Radiat. Res.*, **119**, 219–231.
9. Bonicel,A., Mariaggi,N., Hughes,E. and Téoule,R. (1980) In vitro gamma irradiation of DNA: identification of radioinduced chemical modifications of the adenine moiety. *Radiat. Res.*, **83**, 19–26.
10. Olinski,R., Zastawny,T., Budzbon,J., Skokowski,J., Zegarski,W. and Dizdaroglu,M. (2002) DNA base modifications in chromatin of human cancerous tissues. *FEBS Lett.*, **309**, 193–198.
11. Jałoszyński,P., Jaruga,P., Olinski,R., Biczysko,W., Szyfter,W., Nagy,E., Möller,L. and Szyfter,K. (2003) Oxidative DNA base modifications and polycyclic aromatic hydrocarbon DNA adducts in squamous cell carcinoma of larynx. *Free Radic. Res.*, **37**, 231–240.
12. Girard,P.M., D'Ham,C., Cadet,J. and Boiteux,S. (1998) Opposite base-dependent excision of 7, 8-dihydro-8-oxoadenine by the Ogg1 protein of Saccharomyces cerevisiae. *Carcinogenesis*, **19**, 1299–1305.
13. Jensen,A., Calvayrac,G., Karahalil,B., Bohr,V.A. and Stevnsner,T. (2003) Mammalian 8-oxoguanine DNA glycosylase 1 incises 8-oxoadenine opposite cytosine in nuclei and mitochondria, while a different glycosylase incises 8-oxoadenine opposite guanine in nuclei. *J. Biol. Chem.*, **278**, 19541–19548.
14. Grin,I.R., Dianov,G.L. and Zharkov,D.O. (2010) The role of mammalian NEIL1 protein in the repair of 8-oxo208;7, 8-dihydroadenine in DNA. *FEBS Lett.*, **584**, 1553–1557.
15. Leonard,G.A., Guy,A., Brown,T., Téoule,R. and Hunter,W.N. (1992) Conformation of guanine-8-oxoadenine base pairs in the crystal structure of d(CGCGAATT(O8A)GCG). *Biochemistry*, **31**, 8415–8420.
16. Wood,M.L., Esteve,A., Morningstar,M.L., Kuziemko,G.M. and Essigmann,J.M. (1992) Genetic effects of oxidative DNA damage: comparative mutagenesis of 7, 8-dihydro-8-oxoguanine and 7, 8-dihydro-8-oxoadenine in Escherichia coli. *Nucleic Acids Res.*, **20**, 6023–6032.
17. Kamiya,H., Miura,H., Murata-Kamiya,N., Ishikawa,H., Sakaguchi,T., Inoue,H., Sasaki,T., Masutani,C., Hanaoka,F. and Nishimura,S. (1995) 8-Hydroxyadenine (7, 8-dihydro-8-oxoadenine) induces misincorporation in in vitro DNA synthesis and mutations in NIH 3T3 cells. *Nucleic Acids Res.*, **23**, 2893–2899.
18. Tan,X. (1999) Comparison of the mutagenic properties of 8-oxo-7, 8-dihydro-2'-deoxyadenosine and 8-oxo-7, 8-dihydro-2'-deoxyguanosine DNA lesions in mammalian cells. *Carcinogenesis*, **20**, 2287–2292.
19. Guschlbauer,W., Duplaa,A.M., Guy,A., Téoule,R. and Fazakerley,G.V. (1991) Structure and in vitro replication of DNA templates containing 7, 8-dihydro-8-oxoadenine. *Nucleic Acids Res.*, **19**, 1753–1758.
20. Duarte,V., Muller,J.G. and Burrows,C.J. (1999) Insertion of dGMP and dAMP during in vitro DNA synthesis opposite an oxidized form of 7, 8-dihydro-8-oxoguanine. *Nucleic Acids Res.*, **27**, 496–502.
21. Koag,M.C., Jung,H. and Lee,S. (2019) Mutagenic Replication of the Major Oxidative Adenine Lesion 7, 8-Dihydro-8-oxoadenine by Human DNA Polymerases. *J. Am. Chem. Soc.*, **141**, 4584–4596.
22. Ling,H., Boudsocq,F., Plosky,B.S., Woodgate,R. and Yang,W. (2003) Replication of a cis-syn thymine dimer at atomic resolution. *Nature*, **424**, 1083–1087.
23. Silverstein,T.D., Johnson,R.E., Jain,R., Prakash,L., Prakash,S. and Aggarwal,A.K. (2010) Structural basis for the suppression of skin cancers by DNA polymerase η. *Nature*, **465**, 1039–1043.
24. Zhao,Y., Biertümpfel,C., Gregory,M.T., Hua,Y.-J., Hanaoka,F. and Yang,W. (2012) Structural basis of human DNA polymerase η-mediated chemoresistance to cisplatin. *Proc. Natl. Acad. Sci. U.S.A.*, **109**, 7269–7274.
25. Alt,A., Lammens,K., Chiocchini,C., Lammens,A., Pieck,J.C., Kuch,D., Hopfner,K.-P. and Carell,T. (2007) Bypass of DNA lesions generated during anticancer treatment with cisplatin by DNA polymerase eta. *Science*, **318**, 967–970.
26. Patra,A., Nagy,L.D., Zhang,Q., Su,Y., Müller,L., Guengerich,F.P. and Egli,M. (2014) Kinetics, structure, and mechanism of 8-Oxo-7, 8-dihydro-2′-deoxyguanosine bypass by human DNA polymerase η. *J. Biol. Chem.*, **289**, 16867–16882.
27. Pence,M.G., Choi,J.Y., Egli,M. and Guengerich,F.P. (2010) Structural basis for proficient incorporation of dTTP opposite O6-Methylguanine by human DNA polymerase. *J. Biol. Chem.*, **285**, 40666–40672.
28. Patra,A., Banerjee,S., Salyard,T.L.J., Malik,C.K., Christov,P.P., Rizzo,C.J., Stone,M.P. and Egli,M. (2015) Structural basis for error-free bypass of the 5-N-Methylformamidopyrimidine-dG lesion by human DNA polymerase η and sulfolobus solfataricus P2 polymerase IV. *J. Am. Chem. Soc.*, **137**, 7011–7014.
29. Rodriguez,G.P., Song,J.B. and Crouse,G.F. (2013) In vivo bypass of 8-oxodG. *PLoS Genet.*, **9**, e1003682.
30. Carlson,K.D. and Washington,M.T. (2005) Mechanism of efficient and accurate nucleotide incorporation opposite 7, 8-Dihydro-8-Oxoguanine by Saccharomyces cerevisiae DNA Polymerase η. *Mol. Cell. Biol.*, **25**, 2169–2176.
31. Haracska,L., Yu,S.L., Johnson,R.E., Prakash,L. and Prakash,S. (2000) Efficient and accurate replication in the presence of 7, 8-dihydro-8-oxoguanine by DNA polymerase eta. *Nat. Genet.*, **25**, 458–461.
32. Yuan,F., Zhang,Y., Rajpal,D.K., Wu,X., Guo,D., Wang,M., Taylor,J.S. and Wang,Z. (2000) Specificity of DNA lesion bypass by the yeast DNA polymerase eta. *J. Biol. Chem.*, **275**, 8233–8239.

33. Sabouri,N., Viberg,J., Goyal,D.K., Johansson,E. and Chabes,A. (2008) Evidence for lesion bypass by yeast replicative DNA polymerases during DNA damage. *Nucleic Acids Res.*, **36**, 5660–5667.
34. McCulloch,S.D., Kokoska,R.J., Garg,P., Burgers,P.M. and Kunkel,T.A. (2009) The efficiency and fidelity of 8-oxo-guanine bypass by DNA polymerases delta and eta. *Nucleic Acids Res.*, **37**, 2830–2840.
35. Malins,D.C., Polissar,N.L., Ostrander,G.K. and Vinson,M.A. (2000) Single 8-oxo-guanine and 8-oxo-adenine lesions induce marked changes in the backbone structure of a 25-base DNA strand. *Proc. Natl. Acad. Sci. U.S.A.*, **97**, 12442–12445.
36. Hoppins,J.J., Gruber,D.R., Miears,H.L., Kiryutin,A.S., Kasymov,R.D., Petrova,D.V., Endutkin,A.V., Popov,A.V., Yurkovskaya,A.V., Fedechkin,S.O. *et al.* (2016) 8-Oxoguanine affects DNA backbone conformation in the EcoRI recognition site and inhibits its cleavage by the enzyme. *PLoS One*, **11**, e0164424.
37. Emsley,P. and Cowtan,K. (2004) Coot: model-building tools for molecular graphics. *Acta Crystallogr. D Biol. Crystallogr.*, **60**, 2126–2132.
38. Adams,P.D., Afonine,P.V., Bunkóczi,G., Chen,V.B., Davis,I.W., Echols,N., Headd,J.J., Hung,L.-W., Kapral,G.J., Grosse-Kunstleve,R.W. *et al.* (2010) PHENIX: a comprehensive Python-based system for macromolecular structure solution. *Acta Crystallogr. D Biol. Crystallogr.*, **66**, 213–221.
39. Davis,I.W., Leaver-Fay,A., Chen,V.B., Block,J.N., Kapral,G.J., Wang,X., Murray,L.W., Arendall,W.B., Snoeyink,J., Richardson,J.S. *et al.* (2007) MolProbity: all-atom contacts and structure validation for proteins and nucleic acids. *Nucleic Acids Res.*, **35**, W375–W383.
40. Beard,W.A., Shock,D.D. and Wilson,S.H. (2004) Influence of DNA structure on DNA polymerase β active site function: extension of mutagenic DNA intermediates. *J. Biol. Chem.*, **279**, 31921–31929.
41. Su,Y., Patra,A., Harp,J.M., Egli,M. and Guengerich,F.P. (2015) Roles of residues Arg-61 and Gln-38 of human DNA polymerase η in bypass of deoxyguanosine and 7,8-dihydro-8-oxo-2′-deoxyguanosine. *J. Biol. Chem.*, **290**, 15921–15933.
42. Boldinova,E.O., Ignatov,A., Kulbachinskiy,A. and Makarova,A.V. (2018) The active site residues Gln55 and Arg73 play a key role in DNA damage bypass by S. cerevisiae Pol η. *Sci. Rep.*, **8**, 10314.
43. Sawaya,M.R., Prasad,R., Wilson,S.H., Kraut,J. and Pelletier,H. (1997) Crystal structures of human DNA polymerase beta complexed with gapped and nicked DNA: evidence for an induced fit mechanism. *Biochemistry*, **36**, 11205–11215.
44. Koag,M.C. and Lee,S. (2018) Insights into the effect of minor groove interactions and metal cofactors on mutagenic replication by human DNA polymerase β. *Biochem. J.*, **475**, 571–585.
45. Batra,V.K., Beard,W.A., Shock,D.D., Krahn,J., Pedersen,L.C. and Wilson,S.H. (2006) Magnesium-induced assembly of a complete DNA polymerase catalytic complex. *Structure*, **14**, 757–766.
46. Batra,V.K., Beard,W.A., Shock,D.D., Pedersen,L.C. and Wilson,S.H. (2008) Structures of DNA polymerase beta with active-site mismatches suggest a transient abasic site intermediate during misincorporation. *Mol. Cell*, **30**, 315–324.
47. Ouzon-Shubeita,H., Baker,M., Koag,M.C. and Lee,S. (2019) Structural basis for the bypass of the major oxaliplatin-DNA adducts by human DNA polymerase η. *Biochem. J.*, **476**, 747–758.
48. Biertümpfel,C., Zhao,Y., Kondo,Y., Ramón-Maiques,S., Gregory,M., Lee,J.Y., Masutani,C., Lehmann,A.R., Hanaoka,F. and Yang,W. (2010) Structure and mechanism of human DNA polymerase η. *Nature*, **465**, 1044–1048.
49. Kunkel,T.A. and Bebenek,K. (2000) DNA replication fidelity. *Annu. Rev. Biochem.*, **69**, 497–529.
50. Kunkel,T.A. (2004) DNA replication fidelity. *J. Biol. Chem.*, **279**, 16895–16898.
51. Echols,H. and Goodman,M.F. (1991) Fidelity mechanisms in DNA replication. *Annu. Rev. Biochem.*, **60**, 477–511.
52. Zhao,Y., Gregory,M.T., Biertümpfel,C., Hua,Y.-J., Hanaoka,F. and Yang,W. (2013) Mechanism of somatic hypermutation at the WA motif by human DNA polymerase η. *Proc. Natl. Acad. Sci. U.S.A.*, **110**, 8146–8151.
53. Washington,M.T., Wolfle,W.T., Spratt,T.E., Prakash,L. and Prakash,S. (2003) Yeast DNA polymerase eta makes functional contacts with the DNA minor groove only at the incoming nucleoside triphosphate. *Proc. Natl. Acad. Sci. U.S.A.*, **100**, 5113–5118.
54. Osheroff,W.P. (1996) Enzyme-DNA interactions required for efficient nucleotide incorporation and discrimination in human DNA polymerase beta. *J. Biol. Chem.*, **271**, 12141–12144.
55. Osheroff,W.P., Beard,W.A. and Wilson,S.H. (1999) Base substitution specificity of DNA polymerase β depends on interactions in the DNA minor groove. *J. Biol. Chem.*, **274**, 20749–20752.
56. Xia,S., Christian,T.D., Wang,J. and Konigsberg,W.H. (2012) Probing minor groove hydrogen bonding interactions between RB69 DNA polymerase and DNA. *Biochemistry*, **51**, 4343–4353.
57. Morales,J.C. and Kool,E.T. (1999) Minor groove interactions between polymerase and DNA: more essential to replication than Watson–Crick hydrogen bonds? *J. Am. Chem. Soc.* **121**, 2323–2324.
58. Freudenthal,B.D., Beard,W.A. and Wilson,S.H. (2013) DNA polymerase minor groove interactions modulate mutagenic bypass of a templating 8-oxoguanine lesion. *Nucleic. Acids. Res.*, **41**, 1848–1858.
59. Batra,V.K., Beard,W.A., Hou,E.W., Pedersen,L.C., Prasad,R. and Wilson,S.H. (2010) Mutagenic conformation of 8-oxo-7, 8-dihydro-2′-dGTP in the confines of a DNA polymerase active site. *Nat. Struct. Mol. Biol.*, **17**, 889–890.
60. Koag,M.C., Nam,K. and Lee,S. (2014) The spontaneous replication error and the mismatch discrimination mechanisms of human DNA polymerase β. *Nucleic Acids Res.*, **42**, 11233–11245.